



Published in final edited form as:

Oncogene. 2017 October 19; 36(42): 5852–5860. doi:10.1038/onc.2017.180.

OncoPPI-informed discovery of Mitogen-Activated Protein Kinase Kinase 3 as a novel binding partner of c-Myc

Andrei A. Ivanov^{1,*}, Valentina Gonzalez-Pecchi¹, Layla F. Khuri¹, Qiankun Niu¹, Yifeng Wang¹, Yiran Xu¹, Yan Bai¹, Xiu-Lei Mo¹, Edward V. Prochownik³, Margaret A. Johns¹, Yuhong Du^{1,2}, Fadlo R. Khuri^{1,2}, and Haiyan Fu^{1,2,*}

¹Department of Pharmacology and Emory Chemical Biology Discovery Center, Emory University, Atlanta, GA 30322, USA

²Winship Cancer Institute, Emory University, Atlanta, GA 30322, USA

³Section of Hematology/Oncology, Children's Hospital of Pittsburgh of UPMC and The University of Pittsburgh Cancer Institute, Pittsburgh, PA 15224, USA

Abstract

Mitogen-activated protein kinase kinase 3 (MKK3) is a dual threonine/tyrosine protein kinase that regulates inflammation, proliferation and apoptosis through specific phosphorylation and activation of the p38 MAPK. However, the role of MKK3 beyond p38-signaling remains elusive. Recently, we reported a protein-protein interaction (PPI) network of cancer-associated genes, termed OncoPPI, as a resource for the scientific community to generate new biological models. Analysis of the OncoPPI connectivity identified MKK3 as one of the major hub proteins in the network. Here, we show that MKK3 interacts with a large number of proteins critical for cell growth and metabolism, including the major oncogenic driver MYC. Multiple complementary approaches were employed to demonstrate the direct interaction of MKK3 with MYC *in vitro* and *in vivo*. Computational modeling and experimental studies mapped the interaction interface to the MYC helix-loop-helix domain and a novel 15-residue MYC-binding motif in MKK3 (MBM). The MBM in MKK3 is distinct from the known binding sites for p38 or upstream kinases. Functionally, MKK3 stabilized MYC protein, enhanced its transcriptional activity and increased expression of MYC-regulated genes. The defined MBM peptide mimicked the MKK3 effect in promoting MYC activity. Together, the exploration of OncoPPI led to a new biological model in which MKK3 operates by two distinct mechanisms in cellular regulation through its phosphorylation of p38 and its activation of MYC through protein-protein interaction.

Users may view, print, copy, and download text and data-mine the content in such documents, for the purposes of academic research, subject always to the full Conditions of use: http://www.nature.com/authors/editorial_policies/license.html#terms

*Corresponding authors: Haiyan Fu, Ph. D, Department of Pharmacology, Emory University School of Medicine, 1510 Clifton Road, Atlanta, GA 30322; hfu@emory.edu, Phone: +1-404-275-0368, Fax: +1-404-275-0365; Andrei A. Ivanov, Ph. D, Department of Pharmacology, Emory University School of Medicine, 1510 Clifton Road, Atlanta, GA 30322; andrey.ivanov@emory.edu, Phone: +1-404-727-6343, Fax: +1-404-275-0365;

Conflict of interest

The authors declare no conflict of interest.

Supplementary Information accompanies the paper on the *Oncogene* website (<http://www.nature.com/onc>)

Keywords

protein-protein interaction; oncogenic signaling; MKK3; MYC

Introduction

Recent advances in high-throughput technologies and cancer genomics have led to comprehensive profiling of the cancer genome and identification of genes frequently altered in cancer patients (1–3). To systematically reveal protein-protein interactions (PPIs) among cancer associated proteins, we initiated a binary PPI high-throughput screening (HTS) effort in lung cancer cells (4). The HTS-based studies have led to a dataset with a network of cancer-associated protein-protein interactions (OncoPPI), which are available through the Dashboard and DataPortal of the Cancer Target Discovery and Development (CTD²) Network at the National Cancer Institute (5).

One of the major hubs discovered in the OncoPPI is the mitogen-activated protein kinase kinase 3 (MAP2K3, MKK3). MKK3 is a mitogenic and stress activated dual specificity protein kinase known to specifically phosphorylate and activate p38 MAPK leading to cytokine and chemokine release (6, 7). The p38 pathway is known for its critical role in inflammation, and is involved in regulation of the cell cycle and apoptosis (6). However, the identification of MKK3 as a major hub protein of the OncoPPI was notable due to limited knowledge of its function beyond the regulation of the p38-mediated signaling pathway. Among the MKK3 associated proteins, MYC represents a major oncogene driver, offering an opportunity to define new mechanisms of MKK3 function.

Here, we report a new biological model for MKK3 as a novel regulator of MYC oncogene. This study illustrates an application of the OncoPPI as a resource for the community to generate novel biological models based on the newly detected physical interactions between cancer-associated proteins.

Results

MKK3 interacts with diverse cellular signaling proteins

Analysis of the OncoPPI network revealed that MKK3, but not its close homologue MKK6, interacts with multiple proteins from various signaling pathways, in addition to its known activator, ASK1, and substrate, p38 (Fig. 1A, Fig. S1A) (4). To confirm these interactions, we selected ten positive MKK3 PPIs for examination by TR-FRET titration assay (Fig. 1B) and an alternative GST-affinity resin-based pull down assay (Fig. 1C, 1D). Indeed, both the TR-FRET assay and the GST-pull down assay supported the interaction of MKK3 with these new partners. These MKK3-binding proteins include the Ser/Thr kinase 11 (STK11), cyclin dependent kinase 4 (CDK4) and aurora kinase A (AURKA); the autophagy regulator, Beclin 1; the angiogenesis modulator hypoxia-inducible factor 1-beta (HIF1 β); several membrane associated growth factor receptors including Ephrin type-A receptor 2 (EPHA2), fibroblast growth factor receptor 4 (FGFR4) and platelet-derived growth factor receptor alpha

(PDGFRA) (Fig. 1D); Hippo signaling regulatory protein RASSF1 and the c-MYC (MYC) oncoprotein.

To assess a potential functional connection between MKK3 and its demonstrated binding partners, we examined cancer genomics data (<http://cancergenome.nih.gov>) and performed mutual exclusivity (ME) analysis (8) with datasets from 11 tumor types (Table S1, Fig. S2). Consistent with established pathway connectivity, ME analysis showed a strong tendency toward ME for MKK3 and its known substrate p38 (MAPK14) in all tumor types studied (Table S1). Similarly, MKK3 alterations showed a tendency toward ME with amplifications of FGFR4, EPHA2, PDGFRA, CDK4, and AURKA as well as mutations or deletions of STK11 and RASSF1. Alterations in the HIF1 β coding gene ARNT tend to be mutually exclusive with MKK3 in breast invasive carcinoma (BRCA) and head and neck squamous cell carcinoma (HNSCC). In addition, MKK3 alterations tend to be mutually exclusive with alterations of Beclin1 in HNSCC, as well as in lung adenocarcinoma, prostate adenocarcinoma, liver hepatocellular carcinoma, and sarcoma (Table S1, Fig. S2). Interestingly, ME analysis also revealed the mutual exclusivity of MKK3 alterations with amplification of the MYC oncogene in the majority of the analyzed tumor types (Fig. S2). These genomics data support the functional association of MKK3 with the newly identified interacting proteins, and suggest that MKK3 may play a role in pathways beyond p38. To test this notion, we further examined the physical interaction and functional consequence of the MKK3 interaction with the oncogenic transcription factor MYC.

MKK3 is associated with MYC in cells

To validate the interaction of MKK3 with MYC, a set of PPI detection methods were utilized in addition to the TR-FRET assay. MKK3 was found in complex with MYC in HEK293T cells following GST-pull down with either GST-MKK3 or GST-MYC (Fig. 2A). In agreement with the OncoPPI network, we did not detect the interaction between MYC and MKK6 (Fig. S1B, C). These results further support the high-confident level of the OncoPPI network, and suggest distinct biological functions of MKK3 and MKK6 in the regulation of MYC-driven tumorigenesis. To examine whether the MKK3/MYC interaction occurs under physiological conditions, reciprocal co-immunoprecipitation (co-IP) experiments were performed. Indeed, endogenous MKK3 protein was detected in the MYC protein complex in both H1299 lung cancer cells and MCF7 breast cancer cells (Fig. 2B–D). These results support the physical association of MKK3/MYC in cancer cells.

A Venus-based protein fragment complementation assay (PCA), also known as bimolecular fluorescence complementation assay (BiFC) (9) was employed to monitor subcellular localization of MKK3 when associated with MYC in live cells. The association of two binding partners to the complementary N-terminal and C-terminal fragment of Venus is expected to reconstitute the Venus protein, leading to increased fluorescence intensity (Fig. 2F). Consistent with previous reports, MKK3 and p38 expressed as Venus-fusions in HeLa cells were observed mostly in the cytoplasm, while MYC was in the nucleus (Fig. 2G) (10, 11). As expected, the green fluorescence PCA signal for the MKK3/p38 interaction was observed primarily in the cytoplasm (Fig. 2G). In contrast, the MKK3/MYC PPI was predominantly localized in the nuclei as shown by overlapped fluorescence PCA signal with

Hoechst-stained nuclei (Fig. 2G). Thus, MKK3 appears to form a protein complex with MYC mostly in the nuclear compartment.

In order to bind DNA, MYC forms a high affinity complex with its major binding partner MAX (12). To test if MKK3 also binds to MAX, we performed a TR-FRET assay with the HEK293T cells co-expressing Venus-MKK3/GST-MAX and Venus-MKK3/GST-MYC pairs. In contrast to the MKK3/MYC PPI, we did not observe the interaction between MKK3 and MAX under the same experimental conditions (Fig. 2H). These data further support a specific association of MKK3 with MYC.

MYC helix-loop-helix domain mediates interaction with MKK3

MYC is a master regulator of gene expression that governs a wide range of cellular functions (13). Therefore, its activity is tightly regulated. Such regulatory mechanisms are mediated through a number of defined structural domains in MYC, which couple MYC to MYC-recognition sequences in target DNA, to upstream signaling cascades and to cellular protein degradation machinery (14). These MYC domains and motifs include the conserved MYC-binding domains (MBD) I, II, III and IV in the N-terminal region and a basic-helix-loop-helix leucine zipper (bHLH-LZ) domain at the C-terminal end (14). To identify the region of MYC responsible for MKK3 binding, we examined the interaction of MYC MBD-containing fragments with the full-length MKK3 in TR-FRET and GST-pull down assays (Fig. 3A). As shown in Fig. 3B, the C-terminal 186–439 fragment containing MBIII of MYC was found in complex with GST-MKK3. Considering the significantly decreased binding observed with the 130–338 fragment containing MBIIIa, MBIIIb, and MBIV, these results suggest that the 338–439 binding fragment in the bHLH-LZ region of MYC (Fig. 3A) may serve as the dominant MKK3 binding site. We confirmed this result by using purified GST-MKK3 and His-MYC bHLH-LZ region proteins in a TR-FRET assay. A recombinant GST protein was used as a negative control. The TR-FRET signal for His-MYC bHLH-LZ with GST-MKK3 was 4-fold higher than the signal for the MYC/GST control (Fig. 3C). Then, to assess the affinity of MYC bHLH-LZ to MKK3, the recombinant proteins were subjected to the BioLayer interferometry (BLI) assay (15). BLI is a label-free optical biosensor that measures molecular interactions. For this assay, the His-tagged MYC bHLH-LZ protein bound to the Ni-NTA biosensor was titrated against various concentrations of GST-MKK3 (0 to 300 nM) to generate the BLI signals, leading to the determined dissociation constant of $0.225 \pm 0.005 \mu\text{M}$ (Fig. 3D). This K_d value is comparable to previously reported affinities for various MAP kinases (16, 17) and for the MYC/MAX interaction ($0.167 \pm 0.003 \mu\text{M}$) (18). Together, these results indicate that MYC C-terminal bHLH-LZ domain is the primary interaction site for MKK3.

MKK3 121–135 is a novel interaction domain

A computational molecular modeling approach was utilized to identify a MKK3 domain responsible for MYC binding. First, an MKK3 model was generated based on the crystal structure of its closest homologue MKK6 (Fig. 4A, Fig. S3, Supplementary Information). The correct tertiary structure of MKK3 was validated through computational docking of adenosine triphosphate (ATP), which bound to the MKK3 model with an identical binding mode as has been reported for other MAP kinases (Fig. 4B). In particular, the ATP

phosphate groups were involved in interactions with conserved Lys93 and Lys192 residues, while the adenine ring was located in the kinase hinge region, namely in proximity to Glu141 and Met143.

To predict a putative interface surface for the MKK3/MYC interaction, protein-protein docking was performed using the MKK3 model and the available crystal structure of MYC bHLH-LZ domain (PDB ID: 1NKP) (12). Interestingly, the most energetically favorable complex showed the MYC bHLH-LZ domain fitting within a cavity in a small lobe of MKK3 formed by MKK3 residues 101–160. Computational mutation analysis of MKK3 further indicated that the 121–135 region might be important for MYC binding. Results from a computational alanine scanning experiment predict MKK3 residues Phe121, Leu130, and Phe131 might result in significantly decreased affinity of MKK3 to MYC with only minor effects on overall MKK3 stability (Fig. 4D)

The results of computational modeling were utilized to guide experimental determination of MKK3 MYC-binding domain (Fig 5A). First, MKK3 truncation constructs containing the N-terminal (NTD, residues 1–210) and C-terminal (CT, residues 201–347) fragments of MKK3 were generated (Fig. 5A, 5B). Using a TR-FRET assay, we observed the interaction between full-length MYC and the NTD fragment of MKK3 (Fig. 5C). Then, several smaller fragments of MKK3 NTD were generated and tested, which include MKK3-1-60, 51–110, 101–160, and 101–210. Significant TR-FRET signals were detected for the MYC interaction with full-length, 1–210, 101–210, and 101–160 MKK3 (Fig. 5C). The smallest overlapping region giving a positive signal was a 60 residue fragment of MKK3, fragment 101–160, which appears to serve as the main binding site for MYC (Fig. 5B).

From analysis of the structural model, we identified several structural elements in the MKK3 101–160 fragment (Fig. 5A), including helix C (Ser101-Met115), beta-sheet 4 (Phe121-Asp135), beta-sheet 5 (Asp135-Met140), and helix D (Ser146-Asn158). In order to narrow down the MYC binding domain, short MKK3 peptides within the 101–160 fragment were designed and generated, including a helical peptide 101–115, its longer version 101–121, 101–135 that includes helix C and beta-sheet, and 121–135 corresponding to beta-sheet 4, (Fig. 5A). The fragments of MKK3 were co-expressed as Venus-Flag-tagged fusions with GST-tagged MYC in HEK293T cells and subjected to a GST-pull down assay along with negative controls. A significant band for binding of MYC to MKK3 101–135 and 121–135 peptides was observed compared to the 101–115 and 101–121 fragments, indicating a critical role for MKK3 residues 121–135 in mediating its interaction with MYC (Fig. 5D, 5E). Furthermore, we observed selective binding of the MKK3 101–135 and 121–135 peptides to MYC, compared to MAX or to the known MKK3 binding partners ASK1 and p38 (Fig. 5E, F). Thus, a short, 15 residue MYC-binding peptide containing the MKK3 beta-sheet 4 (Fig. 5A) was identified as a binding site for MYC. This 15 residue region of MKK3 is defined as a MYC binding motif, or MKK3-MBM and was in excellent agreement with the molecular modeling studies shown in Fig. 4. This site is distinct from those previously described as interaction domains with upstream or downstream MAP kinases, ASK1 and p38, representing a new structural element in MKK3 for signaling relay.

MKK3 stabilizes MYC and enhances MYC driven transcription

The data from the above structural analysis further support the interaction between residues 121–135 of MKK3 and the MYC bHLH-LZ domain. Next, we sought to understand if MKK3 binding modulates MYC activity. MYC generally has a short half life in cells that, in part dictates its function (19). Therefore, the impact of MKK3 expression on MYC protein stability was monitored (20, 21). Colon cancer HCT116 cells with relatively high expression levels of endogenous MYC (22, 23) were used to monitor MYC protein levels. While MYC protein was rapidly degraded upon treatment of cells with cycloheximide (CHX), it was significantly stabilized in the presence of MKK3, MKK3 121–135 and ERK1 overexpression (Fig. 6A). Overexpression of Venus had no effect on MYC protein stability. Increased MYC stability in the presence of overexpressed MKK3 was not specific to HCT116 cells, similar effect was observed in MCF7 breast cancer cells (Fig. S4A).

To determine the effect of MKK3 on MYC-transcriptional activity, a luciferase-based MYC transcriptional reporter assay was performed in HEK293T, HCT116, and MCF7 cells (24, 25). Cells were transfected with expression vectors for Venus-MKK3, Venus-MKK3-121–135, Venus-ERK1 (positive control), or Venus alone (negative control) in the presence of a MYC E-box-containing luciferase reporter (Fig. 6B). As expected (13), overexpressed ERK1 increased MYC-driven transcription activity compared to endogenous MYC activity detected with the Venus vector alone. Moreover, overexpression of MKK3 also resulted in increased luminescence of MYC-generated luciferase (Fig. 6B, S4B). Interestingly, overexpression of the artificial MKK3-MBM fragment also increased MYC activity compared to the Venus control (Fig. 6B). MYC is known to stimulate cell proliferation through upregulation of cyclins and cyclin dependent kinases (e.g. CDK4) and suppression of CDK inhibitors such as CDKN1B, CDKN2B, or CDKN2A (26). To determine the effect of MKK3-induced MYC activation on the level of MYC-regulated cell cycle proteins, HCT116 cell lysates expressing MKK3, MKK3 121–135 fragment, or Venus vector were analyzed by Western blotting. Overexpression of MKK3 full length and its MYC-binding domain correlated with increased levels of CCND2 and CDK4 compared to their level in cells expressing Venus alone control (Fig. 6C). Overexpression of MKK3 and MKK3 121–135 consistently led to decreased levels of CDKN1B, confirming MKK3-induced activation of MYC. To further examine the role of MKK3 in the regulation of MYC-induced genes, qRT-PCR was used to monitor the expression level of well-established MYC-driven genes, CDK6 and CDKN2A. Like ERK1, overexpressed MKK3, or MKK3 121–135, increased CDK6 while decreased CDKN2A mRNA levels (Fig. 6D).

Together, our results suggest a novel role for MKK3 as a positive regulator of MYC activity through direct protein-protein interaction.

Discussion

Here, we presented data supporting the interaction of MKK3 with multiple signaling pathway regulators in addition to its known regulators in the stress activated MAPK pathway, ASK1 and p38. These MKK3 partners include CDK4, AURKA, HIF1 β , STK11, RASSF1, Beclin1, and MYC. Although the significance of MKK3 interaction with these proteins remains to be established, our results imply that MKK3 may have a broader role as

a signaling hub than previously recognized. Indeed, our analysis of mutual exclusivity of genomic alterations provides additional support for a functional connection between MKK3 and its novel protein partners, including MYC, in different types of tumors.

MYC is an oncogenic transcription factor that regulates cell growth and proliferation, and its amplification is correlated with poor survival and prognosis of cancer patients (27). MYC has been shown to be regulated by a variety of proteins, including other kinases such as ERKs and GSK3 β . Our work identifies MKK3 as a new MYC regulator. Interestingly, we did not detect the interaction between MYC and MKK6, a close homologue of MKK3, under the same experimental conditions. These data suggest that MKK3 and MKK6 have different functions in the regulation of MYC in cancer cells.

The results of TR-FRET and BLI assays performed with recombinant purified MKK3 and the C-terminal MYC-HLH-LZ, as well as our co-immunoprecipitation experiments, suggest a direct physical interaction between MKK3 and MYC. Mechanistically, MKK3 appears to regulate MYC by inhibiting MYC degradation and enhancing its transcriptional activity. Consistent with this role, overexpression of MKK3 in HCT116 cells is correlated with the upregulation of MYC-regulated genes, CDK4, CDK6, and CCND2, and suppression of CDK inhibitors CDKN1B and CDKN2A. These data suggest a new role for MKK3 as an activator of MYC that enhances MYC-driven cell proliferation. Indeed, knockdown of MKK3 in multiple cancer cell lines has been correlated with suppression of cell proliferation (28).

The MYC-binding site is located at the N-terminal part of MKK3 outside of the kinase domain, which suggests a kinase-independent mechanism for the MKK3/MYC interaction. However, the regulatory function of MKK3 in MYC driven program remains to be established. It remains possible that the kinase activity is required to regulate the MYC associated transcription complex upon recruitment (29, 30).

MKK3 is activated by MAP3K kinases, such as ASK1 or TAK1, which bind to a MKK3 DVD docking site formed by C-terminal residues 311–344 (31). Upon its activation, the MKK3 N-terminal 17–33 fragment binds to p38 leading to its phosphorylation and activation (32). Here, we identified a short fragment (121–135; MBM), located in the central region of MKK3 that binds to MYC. This peptide does not show any significant binding to p38 suggesting a new function for MKK3 in regulation of MYC oncogenic activity aside of p38-activation. Furthermore, our discovery of non-overlapping binding domains in the MKK3 protein for MYC and p38 implies that these different functions of MKK3 could potentially be independently targeted with inhibitors for therapeutic discovery.

In summary, our data reveal MKK3 as a major hub of a cancer protein-protein interaction network and confirm interactions with at least 10 novel binding partners known as key regulators of cell growth, including the master transcriptional regulator MYC. With specific focus on the MKK3/MYC interaction, we demonstrate that MKK3 can upregulate MYC activity in cancer cells. These data strongly support a new mechanism for the control of MYC-driven program through MKK3.

Methods

Cell culture conditions

All cell lines were obtained from the American Type Culture Collection (ATCC, Rockville, MD, USA). Human lung cancer cells H1299 (ATCC CRL-5803) were cultured in Roswell Park Memorial Institute (RPMI) 1640 containing L-glutamine (CORNING Cat# 10-040) supplemented with 10% fetal bovine serum and 1% penicillin/streptomycin solution (CellGro). HEK293T (ATCC CRL-3216), HeLa (ACTT CCL-2), MCF7 (ACTT HTB-22), and HCT116 (ACTT CCL-247) cells (ATCC, Manassas, VA) were maintained in Dulbecco's Modified Eagle's Medium (DMEM), with 4.5 g/L glucose, L-glutamine, and sodium pyruvate (CellGro, Cat# 10-013-CV) supplemented with 10% fetal bovine serum and 1% penicillin/streptomycin solution (CellGro, Cat# 30-002-CI). Cells were incubated at 37°C in humidified conditions with 5% CO₂.

Transfection

For TR-FRET and GST-pull down assays the cells were transfected using 1mg/mL polyethylenimine in a ratio of 3 µL to 1 µg DNA. For MYC-reporter, MYC-stability, and qRT-PCR assays cells were transfected with Xtreme-Gene (Roche Cat# 6366546001) in a ratio of 3 µL to 1 µL g DNA following the manufacturer's instructions.

Time-resolved fluorescence resonance energy transfer (TR-FRET)

Test proteins were expressed for 48 h in HEK293T cells. Cell lysates were prepared in the 1% NP-40 Lysis buffer (150 mM NaCl, 10 mM HEPES pH 7.5, 1% nonident P-40 (IGEPAL CA-630, Sigma-Aldrich), 5 mM sodium pyrophosphate, 5 mM NaF, 2 mM sodium orthovanadate, 10 mg/L aprotinin, 10 mg/L leupeptin and 1mM PMSF) for 30 min at 4 °C, followed by 15 min centrifugation at 14,000 RPM at 4°C. The TR-FRET assay was performed in the Reaction buffer (20 mM Tris-HCl pH 7.0, 50 mM NaCl, 0.01% NP-40) in 384-well black plates. GST-Terbium-conjugated antibody (Cisbio Bioassays 61GSTTLB, 1:1000 dilution) was used to couple GST-tagged protein as a FRET donor. Venus-tagged proteins served as a FRET acceptor.

For the TR-FRET assay with recombinant proteins, 6 nM recombinant GST-MKK3 protein was mixed with 50 nM recombinant His-MYC-bHLH-LZ protein in the Reaction buffer and the reactions were carried out as described above. Samples were incubated at room temperature for 1 h in 384-well plate, and the FRET signal was measured on the Envision spectrophotometer with the following settings: setting: Ex 337 nm, Em1: 520 nm, Em2: 486 nm; mirror: D400/D505 dual; time delay: 50 us). The TR-FRET signal is expressed as the FRET ratio ($520_{\text{nm}}/486_{\text{nm}} \times 10^4$).

Bio-layer interferometry (BLI) assay

Binding studies were carried out using the Octet Red 384 system (Forte Bio), at 30 °C with shaking at 1500 RPM in a 384-well plate containing 50 µl of the solution in each well. 1X BLI Kinetic Buffer (PBS, pH 7.4, 10 mg/ml bovine serum albumin (BSA) and 0.1% (v/v) Tween 20) was used throughout this study for protein dilution and washing steps. Ni-NTA biosensors were balanced for the first baseline and then loaded with poly-histidine tagged

MYC peptide (50 µg/ml) followed by another wash for the second baseline. Kinetic analysis of the MYC-MKK3 interaction was performed by dipping the sensors into the well containing GST-MKK3 (0 to 300 nM). The maximum change in light interference in the association step was determined for each GST-MKK3 concentration (using the second baseline value), and a standard curve was plotted using one-site binding (hyperbola) nonlinear regression.

GST-pull down, co-immunoprecipitation, and western blot analysis

The GST-pull down and co-immunoprecipitation assays were performed as previously described (4). For the GST-pull down assays, cells were lysed in the 1% NP-40 Lysis buffer and incubated with glutathione-conjugated beads (GE 17527901) for 2 h at 4 °C. Beads were washed three times with the 1% NP-40 Lysis buffer and eluted by boiling in sodium dodecyl sulfate-polyacrylamide gel electrophoresis (SDS-PAGE) loading buffer. For co-immunoprecipitation (co-IP), cells were lysed with 0.5% NP-40 Lysis buffer as previous described to extract both, cytoplasmic and nuclear proteins, including MYC (33). Cell lysates were collected and cleared by centrifugation at 14,000 RPM at 4 °C for 10 min. The cleared lysates (1.5–2 mg of total proteins) were mixed with protein G-beads (20 µL) for 1h to remove non-specific binding proteins. Then, the cleared supernatants were transferred to clean tubes, mixed with MKK3 antibody (10 µg; Santa Cruz sc135985), or MYC antibody (4 µg Abcam, ab17355), or IgG control (Santa Cruz sc-2025), and incubated at 4 °C overnight. Next day, the samples were incubated with protein G-beads (20 µL) for 2 h at 4°C. Immunoprecipitates were washed three times with 500 µl of the Lysis buffer. The immunocomplexes were eluted with SDS-PAGE sample buffer and analyzed by Western blotting with indicated antibodies.

Antibodies

The following antibodies were used for the western blotting: MYC (Cell signaling 5605S, 1:1000 dilution), γ -tubulin (Sigma T-5326, 1:2000 dilution), Flag-HRP (Sigma A8592, 1:1000 dilution), GST-HRP (Sigma A7340, 1:1000 dilution), MKK3 (Santa Cruz sc-961, 1:1000 dilution), MYC (Cell signaling 5605S, 1:1000 dilution), GAPDH (Cell Signaling 2118, 1:1000 dilution), CDKN1B (p27, Cell Signaling 2552, 1:1000 dilution), CCND2 (Cell Signaling 3741P, 1:1000 dilution), CDK4 (Santa Cruz sc-260, 1:1000 dilution).

Protein Fragment Complementation Assay (PCA) and cell imaging

The cells were co-transfected with MKK3 and MYC or p38 conjugated to C-terminal or N-terminal fragments of Venus. The cells transfected with individual plasmids served as a control. Proteins were expressed for 48 h, and the protein-protein interactions were monitored in live cells based on the fluorescence intensity of reconstituted Venus. The cell nuclei were stained with the Hoechst 33342 5µg/ml solution (ThermoFisher, cat# H3570) for 30 minutes at 4° C. The cell images were taken with ImageXpress system at 447nm (Hoechst nuclei stain) and 530nm (Venus green fluorescence). The fluorescence intensity of reconstituted Venus was measured on the Envision spectrophotometer (Ex 485 nM and Em 535 nm, mirror 505 nm).

Protein stability assay

The proteins were expressed for 24h and then serum starved for an additional 24h. Then, cells were treated with 100 µg/mL cycloheximide (Cell Signaling, cat# 2112). At the indicated times, 100 µl of 2X SDS-PAGE sample buffer was added and the cells were scraped from the wells, and boiled for 5 min. After all lysates were collected, each sample was loaded onto a 10% SDS-PAGE gel and then analyzed by western blotting.

MYC-reporter assay

The MYC transcription activity was measured using MYC-reporter assay (34). Cells were transfected with Venus-Flag-MKK3, Venus-Flag-MKK3-121-135, Venus-Flag-ERK1, or Flag-Venus vector along with Myc-E-box-containing Firefly luciferase reporter plasmid. Renilla luciferase expression vector served as a calibration control. For the dose dependent assay, MCF7 cells were co-transfected with Venus-Flag-MKK3 or Flag-Venus vector at the final concentration of 0 to 0.75 ng/µL. The proteins were expressed in cells for 24 h in DMEM media supplemented with 10% FBS, and then serum starved for 24 h. Then, cells were harvested, and transferred to a 384-well plate (20 µL per well). MYC reporter assay was performed using Dual-Glo luciferase kit (Promega, Cat# E2920) following manufacturer's instructions. The normalized luminescence was calculated as a ratio of luminescence of Firefly luciferase to the luminescence of Renilla luciferase.

Reverse-transcriptase polymerase chain reaction (qRT-PCR)

HCT116 cells transfected with Venus or Venus-tagged MKK3, MKK3 121–135, or ERK1 were incubated for 24 hours in DMEM media supplemented with 10% FBS, and then serum starved for an additional 24h. The mRNA was purified using the RNeasy Mini kit (Qiagen Cat# 74104) following manufacture instructions. Then, to degrade DNA, the mRNA samples were treated with DNase I (Invitrogen, Cat# 18068015) followed by heat inactivation at 65°C for 10 minutes in the presence of 2 mM EDTA. cDNA was synthesized using 250 ng of total RNA and the SuperScript IV first-strand cDNA synthesis kit (Invitrogen, Cat# 18091050). The real-time PCR was performed using SsoAdvanced Universal SYBR Green Supermix reagent (Bio-Rad, Cat#, 172-5271). The delta cycle threshold (Δ Ct) values were calculated by subtraction of GAPDH Ct from test gene Ct. Then, relative mRNA levels were calculated by subtraction of Venus Ct values from test gene Ct values resulting in Δ Ct value, and the fold change was determined as $FC = 2^{-\Delta Ct}$ (35). The primer sequences and the PCR cycling program are indicated in SI.

Cell culture conditions, DNA plasmids, and protein purification

The detailed information is provided in SI.

MKK3 homology modeling and protein-protein docking

The computational modeling was performed using the Schrodinger Suite software (Schrodinger, Cambridge, MA, USA) as described in SI.

Analysis of mutual exclusivity

A mutual exclusivity analysis of genomic alterations of MKK3 and its binding partners was performed with the cBioPortal (36) using TCGA Provisional data sets with sequencing and copy-number alteration data from 11 tumor types (Table S1).

Data analysis

The TR-FRET, BLI, PCA, and qRT-PCR assays were performed and repeated three times. The data quantification was performed using the GraphPad Prism software.

Data availability

The source and IDs of the genes and expression vectors used in the studies are summarized in Supplementary Table 2. All experimental data are available from the authors.

Supplementary Material

Refer to Web version on PubMed Central for supplementary material.

Acknowledgments

We thank Min Qui for technical assistance. We thank Lauren Rusnak for editing the manuscript. This research was supported in part by NIH U01CA168449 (HF) and Winship Cancer Institute (NIH 5P30CA138292), and by Emory University Research Committee 2015 award (A.A.I.). The results published here are in part based upon data generated by the TCGA Research Network: <http://cancergenome.nih.gov/>.

References

1. Tomczak K, Czerwinska P, Wiznerowicz M. The Cancer Genome Atlas (TCGA): an immeasurable source of knowledge. Contemporary oncology (Poznan, Poland). 2015; 19(1A):A68–77.
2. Hudson TJ, Anderson W, Artez A, Barker AD, Bell C, Bernabe RR, et al. International network of cancer genome projects. Nature. 2010; 464(7291):993–8. [PubMed: 20393554]
3. Forbes SA, Beare D, Gunasekaran P, Leung K, Bindal N, Boutselakis H, et al. COSMIC: exploring the world's knowledge of somatic mutations in human cancer. Nucleic acids research. 2015; 43(Database issue):D805–11. [PubMed: 25355519]
4. Li Z, Ivanov AA, Su R, Gonzalez-Pecchi V, Qi Q, Liu S, et al. The OncoPPi network of cancer-focused protein-protein interactions to inform biological insights and therapeutic strategies. Nat Commun. 2017; 8:14356. [PubMed: 28205554]
5. Schreiber SL, Shamji AF, Clemons PA, Hon C, Koehler AN, Munoz B, et al. Towards patient-based cancer therapeutics. Nature biotechnology. 2010; 28(9):904–6.
6. Zarubin T, Han J. Activation and signaling of the p38 MAP kinase pathway. Cell research. 2005; 15(1):11–8. [PubMed: 15686620]
7. Wagner EF, Nebreda AR. Signal integration by JNK and p38 MAPK pathways in cancer development. Nature reviews Cancer. 2009; 9(8):537–49. [PubMed: 19629069]
8. Babur O, Gonen M, Aksoy BA, Schultz N, Ciriello G, Sander C, et al. Systematic identification of cancer driving signaling pathways based on mutual exclusivity of genomic alterations. Genome biology. 2015; 16:45. [PubMed: 25887147]
9. Kodama Y, Hu CD. Bimolecular fluorescence complementation (BiFC): a 5-year update and future perspectives. BioTechniques. 2012; 53(5):285–98. [PubMed: 23148879]
10. Ruzinova MB, Caron T, Rodig SJ. Altered subcellular localization of c-Myc protein identifies aggressive B-cell lymphomas harboring a c-MYC translocation. The American journal of surgical pathology. 2010; 34(6):882–91. [PubMed: 20442643]

11. Ben-Levy R, Hooper S, Wilson R, Paterson HF, Marshall CJ. Nuclear export of the stress-activated protein kinase p38 mediated by its substrate MAPKAP kinase-2. *Current biology: CB*. 1998; 8(19):1049–57. [PubMed: 9768359]
12. Nair SK, Burley SK. X-ray structures of Myc-Max and Mad-Max recognizing DNA. *Molecular bases of regulation by proto-oncogenic transcription factors*. *Cell*. 2003; 112(2):193–205. [PubMed: 12553908]
13. Adhikary S, Eilers M. Transcriptional regulation and transformation by Myc proteins. *Nature reviews Molecular cell biology*. 2005; 6(8):635–45. [PubMed: 16064138]
14. Tu WB, Helander S, Pilstal R, Hickman KA, Lourenco C, Jurisica I, et al. Myc and its interactors take shape. *Biochimica et biophysica acta*. 2015; 1849(5):469–83. [PubMed: 24933113]
15. Sultana A, Lee JE. Measuring protein-protein and protein-nucleic Acid interactions by biolayer interferometry. *Current protocols in protein science*. 2015; 79:19.25.1–6.
16. Bunkoczi G, Salah E, Filippakopoulos P, Fedorov O, Muller S, Sobott F, et al. Structural and functional characterization of the human protein kinase ASK1. *Structure*. 2007; 15(10):1215–26. [PubMed: 17937911]
17. Kragelj J, Palencia A, Nanao MH, Maurin D, Bouvignies G, Blackledge M, et al. Structure and dynamics of the MKK7-JNK signaling complex. *Proceedings of the National Academy of Sciences of the United States of America*. 2015; 112(11):3409–14. [PubMed: 25737554]
18. Banerjee A, Hu J, Goss DJ. Thermodynamics of protein-protein interactions of cMyc, Max, and Mad: effect of polyions on protein dimerization. *Biochemistry*. 2006; 45(7):2333–8. [PubMed: 16475822]
19. Thomas LR, Tansey WP. Proteolytic control of the oncoprotein transcription factor Myc. *Advances in cancer research*. 2011; 110:77–106. [PubMed: 21704229]
20. Pan J, Deng Q, Jiang C, Wang X, Niu T, Li H, et al. USP37 directly deubiquitinates and stabilizes c-Myc in lung cancer. *Oncogene*. 2015; 34(30):3957–67. [PubMed: 25284584]
21. Li S, Jiang C, Pan J, Wang X, Jin J, Zhao L, et al. Regulation of c-Myc protein stability by proteasome activator REGgamma. *Cell Death Differ*. 2015; 22(6):1000–11. [PubMed: 25412630]
22. Sun XX, He X, Yin L, Komada M, Sears RC, Dai MS. The nucleolar ubiquitin-specific protease USP36 deubiquitinates and stabilizes c-Myc. *Proceedings of the National Academy of Sciences of the United States of America*. 2015; 112(12):3734–9. [PubMed: 25775507]
23. Parajuli P, Tiwari RV, Sylvester PW. Anti-proliferative effects of gamma-tocotrienol are associated with suppression of c-Myc expression in mammary tumour cells. *Cell proliferation*. 2015; 48(4): 421–35. [PubMed: 26096843]
24. Jung KY, Wang H, Teriete P, Yap JL, Chen L, Lanning ME, et al. Perturbation of the c-Myc-Max protein-protein interaction via synthetic alpha-helix mimetics. *Journal of medicinal chemistry*. 2015; 58(7):3002–24. [PubMed: 25734936]
25. Yin X, Giap C, Lazo JS, Prochownik EV. Low molecular weight inhibitors of Myc-Max interaction and function. *Oncogene*. 2003; 22(40):6151–9. [PubMed: 13679853]
26. Bretones G, Delgado MD, Leon J. Myc and cell cycle control. *Biochimica et biophysica acta*. 2015; 1849(5):506–16. [PubMed: 24704206]
27. Lin CY, Loven J, Rahl PB, Paranal RM, Burge CB, Bradner JE, et al. Transcriptional amplification in tumor cells with elevated c-Myc. *Cell*. 2012; 151(1):56–67. [PubMed: 23021215]
28. Baldari S, Ubertaini V, Garufi A, D’Orazi G, Bossi G. Targeting MKK3 as a novel anticancer strategy: molecular mechanisms and therapeutical implications. *Cell death & disease*. 2015; 6:e1621. [PubMed: 25633290]
29. Chymkowitz P, Eldholm V, Lorenz S, Zimmermann C, Lindvall JM, Bjoras M, et al. Cdc28 kinase activity regulates the basal transcription machinery at a subset of genes. *Proceedings of the National Academy of Sciences of the United States of America*. 2012; 109(26):10450–5. [PubMed: 22689984]
30. Zippo A, De Robertis A, Serafini R, Oliviero S. PIM1-dependent phosphorylation of histone H3 at serine 10 is required for MYC-dependent transcriptional activation and oncogenic transformation. *Nat Cell Biol*. 2007; 9(8):932–44. [PubMed: 17643117]

31. Takekawa M, Tatebayashi K, Saito H. Conserved docking site is essential for activation of mammalian MAP kinase kinases by specific MAP kinase kinase kinases. *Molecular cell*. 2005; 18(3):295–306. [PubMed: 15866172]
32. Cuadrado A, Nebreda AR. Mechanisms and functions of p38 MAPK signalling. *Biochem J*. 2010; 429(3):403–17. [PubMed: 20626350]
33. Ponzielli R, Tu WB, Jurisica I, Penn LZ. Identifying Myc interactors. *Methods in molecular biology* (Clifton, NJ). 2013; 1012:51–64.
34. Gupta S, Seth A, Davis RJ. Transactivation of gene expression by Myc is inhibited by mutation at the phosphorylation sites Thr-58 and Ser-62. *Proceedings of the National Academy of Sciences of the United States of America*. 1993; 90(8):3216–20. [PubMed: 8386367]
35. Livak KJ, Schmittgen TD. Analysis of relative gene expression data using real-time quantitative PCR and the 2⁻(Delta Delta C(T)) Method. *Methods* (San Diego, Calif). 2001; 25(4):402–8.
36. Gao J, Aksoy BA, Dogrusoz U, Dresdner G, Gross B, Sumer SO, et al. Integrative analysis of complex cancer genomics and clinical profiles using the cBioPortal. *Science signaling*. 2013; 6(269):p11. [PubMed: 23550210]

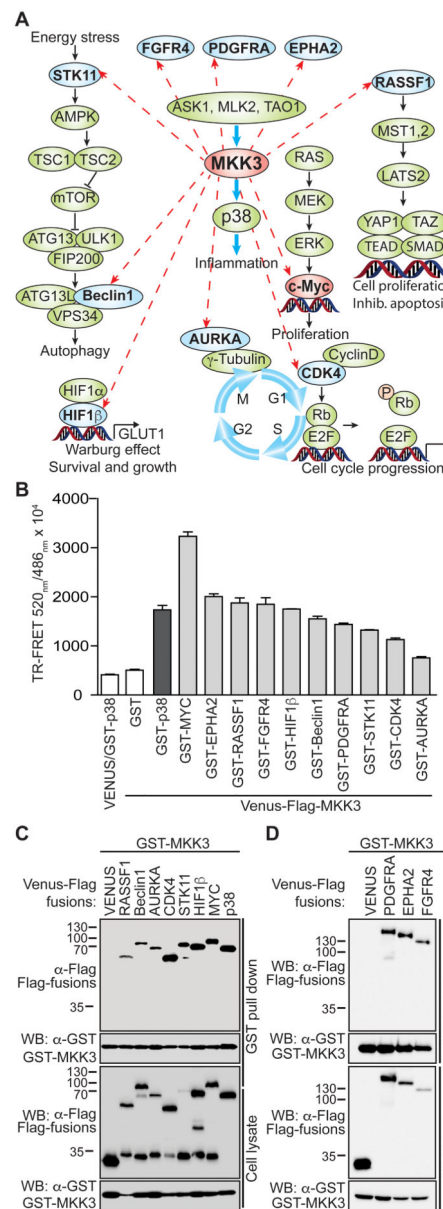


Figure 1. MKK3 interacts with proteins beyond p38

A) Diagram showing new MKK3 binding partners and associated pathways. B) Validation of the MKK3 interaction with partners in a TR-FRET assay. The TR-FRET assay was performed for Venus-Flag-tagged MKK3 co-expressed in HEK293T cells with GST-fusions (light grey bars). Venus-Flag-MKK3/GST and GST-p38/Venus were included as negative controls (white bars), Venus-Flag-MKK3/GST-p38 served as a positive control (dark grey bar). The data was obtained in triplicate, bars represent averaged TR-FRET signals expressed as the FRET ratio (520_{nm}/486_{nm} × 10⁴). C) The interactions of MKK3 with its partners were validated in a GST-pull down assay performed for GST-MKK3 co-expressed in HEK293T cells with Venus-Flag fusions. Venus-Flag-tagged p38 and Flag-Venus alone served as positive and negative controls for the assay.

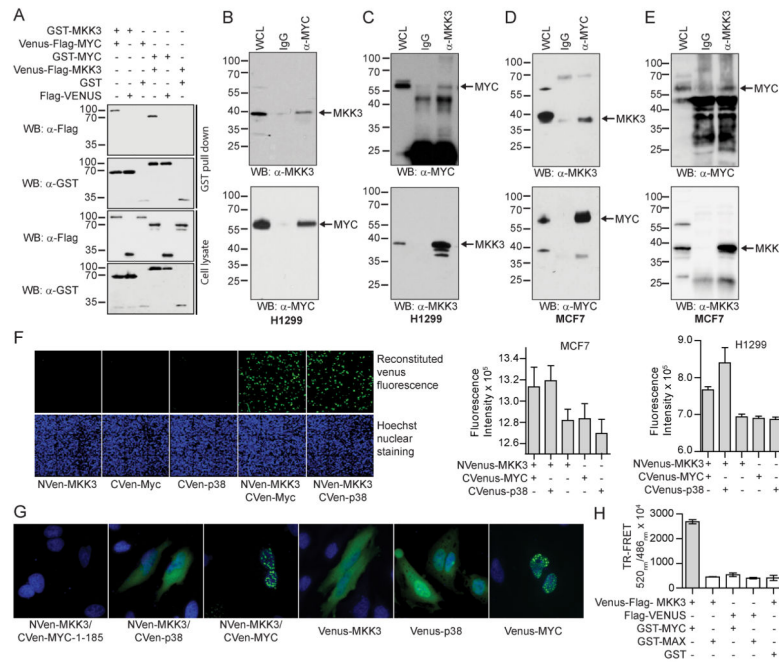


Figure 2. MKK3 is a novel binding partner of MYC

A) MKK3 interacts with MYC in reciprocal GST-pull down assays. The assay was performed in HEK293T cells expressing GST- and Venus-Flag-tagged MKK3 and MYC. GST and Flag-Venus alone served as negative controls. B) Endogenous co-immunoprecipitation (co-IP) of MKK3 with MYC in lung cancer H1299 cells. Mouse IgG was used as a negative control for the assay. C) Endogenous co-IP of MYC with MKK3 in H1299 cells. D) Endogenous co-IP of MKK3 with MYC in breast cancer MCF7 cells. E) Endogenous co-IP of MYC with MKK3 in MCF7 cells. F) MKK3 interact with MYC in live H1299 and MCF7 cells. The left panel shows a representative image of MCF7 cells producing green fluorescence of reconstituted Venus observed for MKK3 conjugated with N-terminal part of Venus (NVen-MKK3) overexpressed with MYC or p38 conjugated with Venus C-terminal (CVen) part of Venus protein (CVenus) but not for individually transfected proteins. Hoechst nuclei staining is shown in blue. The bars on the right side represent green fluorescence of reconstituted Venus detected in triplicate in MCF7 and H1299 cells. G) MKK3 interacts with MYC in nucleus. NVen-MKK3 was co-expressed in HeLa cells with CVenus-p38 or CVenus-MYC along with Venus-MKK3, Venus-p38, and Venus-MYC expressed individually and the Venus green fluorescence was monitored. The Hoechst nuclei staining is shown in blue. Venus-MKK3, and Venus-p38 were mostly expressed in the cytoplasm. Venus-MYC preferably expressed in the nuclei. MKK3/p38 PPI was observed mostly in the cytoplasm. In contrast, MKK3/MYC interaction was observed in the nuclei. MYC 1–185 fragment was included as a negative control. H) MKK3 failed to bind MAX, a MYC binding partner. TR-FRET assay performed for Venus-Flag-MKK3 co-expressed with GST-tagged MYC or MAX in HEK293T cells. The bars represent averaged TR-FRET ratio obtained in triplicate.

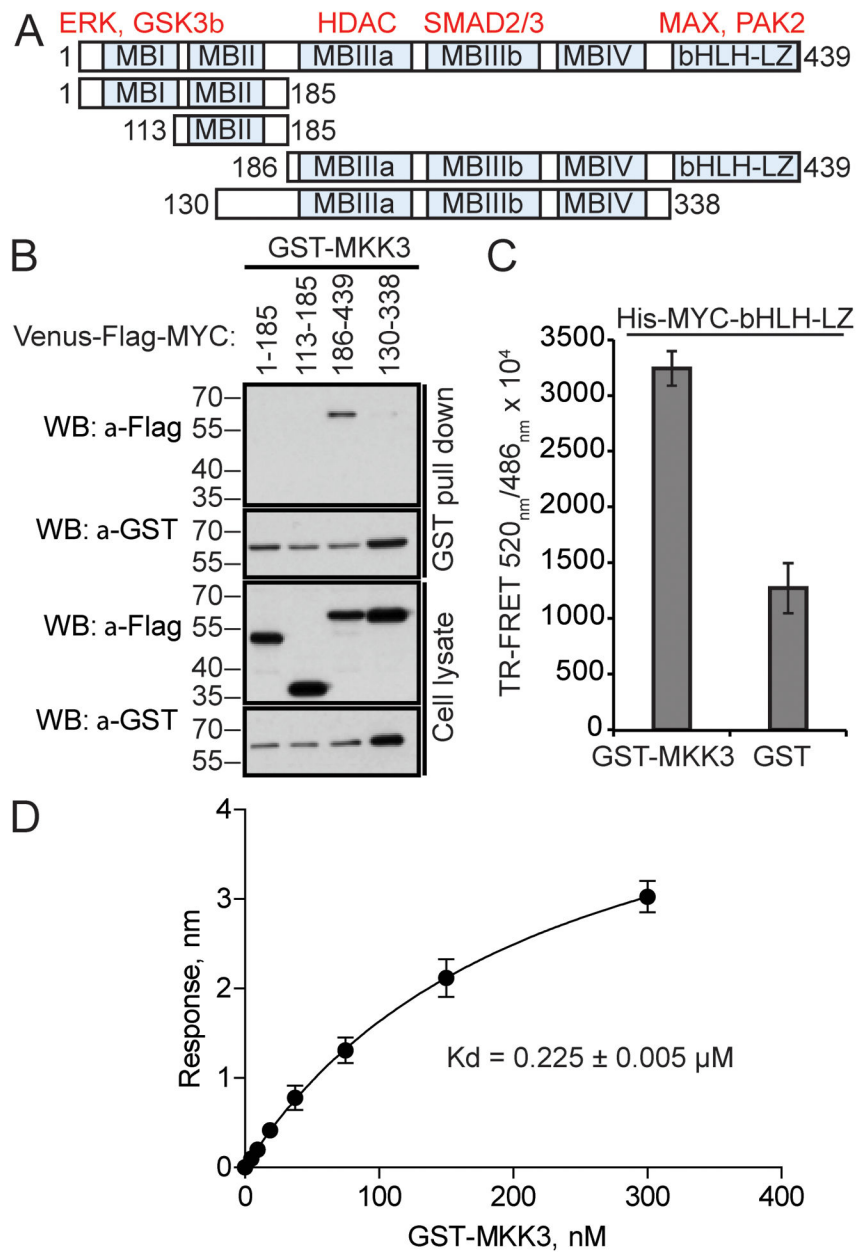


Figure 3. MKK3 binds to MYC bHLH-LZ domain

A) MYC fragments generated to map its MKK3-binding site. Examples of MYC binding partners are shown in red above defined MYC domains (MB). B) MKK3 preferably binds to MYC 186–439 region in GST-pull down assay performed in HEK293T cells with GST-MKK3 co-expressed with Venus-Flag-MYC fragments. C) MYC bHLH-LZ domain is sufficient for MKK3 binding in vitro. Recombinant GST-MKK3 and His-MYC-bHLH-LX proteins were used in a TR-FRET assay. Recombinant GST protein was used as a negative control. TR-FRET signal was measured in triplicate. D) The interaction between recombinant GST-MKK3 and His-MYC-bHLH-LZ was detected using the Bio-layer interferometry assay. The maximum change in light interference in the association step was

determined for indicated concentrations of GST-MKK3. A standard curve was plotted using one-site binding (hyperbola) nonlinear regression. The error bars indicate standard deviation of three independent experiments.

Author Manuscript

Author Manuscript

Author Manuscript

Author Manuscript

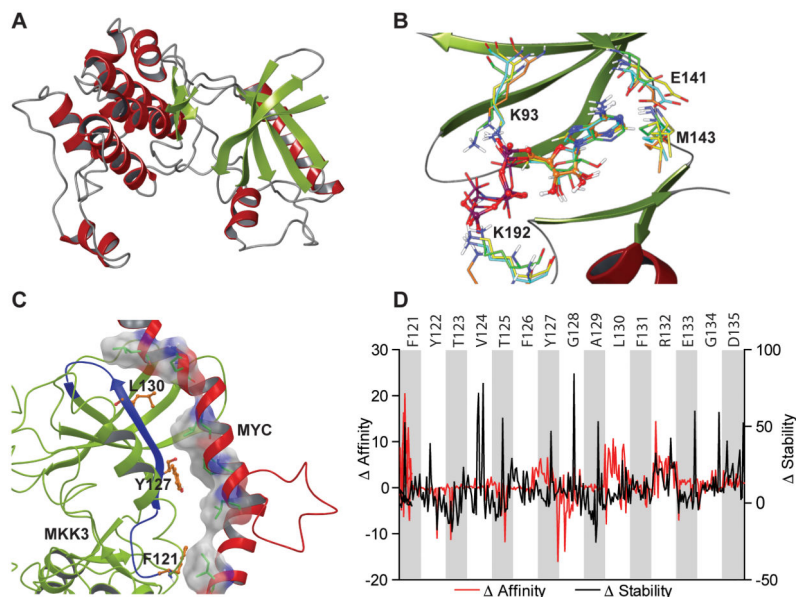


Figure 4. Computational modeling predicted MKK3 MYC-binding domain

A) A computational homology model of MKK3 was constructed based on the crystal structure of MKK6. B) Superimposition of ATP docked to MKK3 model (orange) with ATP extracted from the crystal structures of MKK4 (green), MEK1 (yellow), and MEK2 (cyan). The results of molecular docking revealed the same binding mode of ATP at MKK3 as observed in the crystal structures solved for other kinases. C) A model of MYC HLH domain bound to MKK3. The results of protein-protein docking predicted MKK3 121–135 fragment as a main MKK3 MYC-binding domain. MYC shown in red, MKK3 shown in green, MKK3 121–135 fragment is highlighted in blue. D) An impact of MKK3 121–135 residues on MKK3 stability and MKK3/MYC binding affinity was evaluated with a computational mutagenesis. The results suggest that alanine mutations of MKK3 F121, Y127, and L130 (shown in orange in panel C) significantly decrease MYC binding affinity with a minor effect on overall MKK3 stability.

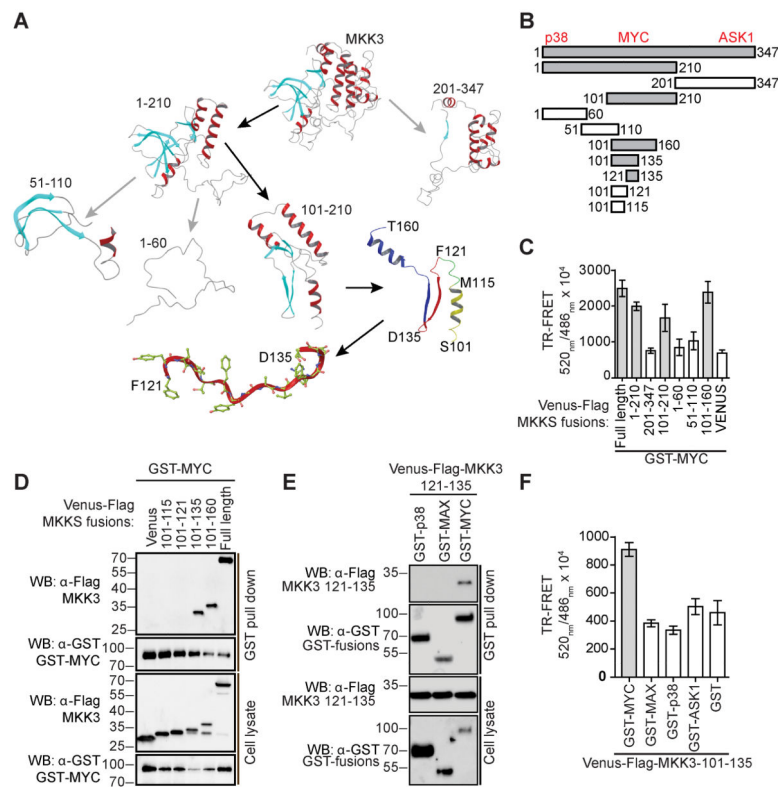


Figure 5. MKK3 121–135 is sufficient for MYC-binding

A) A computational model of MKK3 was utilized to guide the design of truncation fragments. MKK3 MYC-binding fragments are highlighted with black arrows. B) MKK3 fragments were generated to identify MKK3 binding site for MYC. MKK3 MYC-binding regions are shown in grey. Approximate locations of MKK3 sites for p38, ASK1, and MYC are indicated on top. C) Interaction of MYC with fragments of MKK3 in a TR-FRET assay in HEK293T cells. The bars represent average TR-FRET signals measured in triplicate. D) Interaction of MYC with defined peptides of MKK3 in a GST-pull down assay performed in HEK293T cells. E) Interaction of MKK3 121–135 peptide with MYC in a GST-pull down assay in HEK293T cells with p38 and MAX as controls. F) MKK3 101–135 showed selective interaction with MYC in a TR-FRET assay.

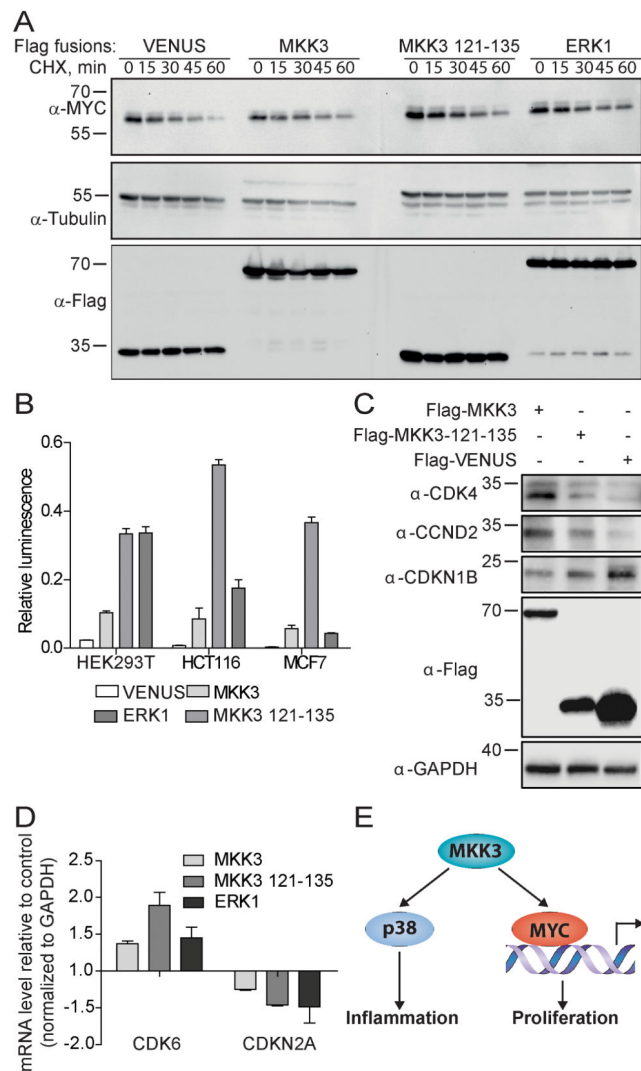


Figure 6. MKK3 inhibits MYC degradation and upregulates its activity

A) MKK3 and MKK3 121–135 MYC-binding peptide inhibit MYC degradation in HCT116 cells. HCT116 cells were transfected with Venus-Flag-MKK3, Venus-Flag-MKK3-121-135, Venus-Flag-ERK1, or Flag-Venus alone for 48h and treated with 100 mg/ml cycloheximide (CHX) for indicated times. Western blotting was performed to reveal the level of endogenous MYC. Tubulin was used as a control. B) MKK3 and MKK3 121–135 enhances MYC transcriptional activity in HEK293T, HCT116, and MCF7 cells in MYC luciferase reporter assay. The cells were co-transfected with Venus-Flag-MKK3, Venus-Flag-MKK3-121-135, or Flag-Venus, Firefly luciferase reporter plasmid containing four E-box sites, and Renilla luciferase used as a transfection efficiency control. The MYC-transcriptional activity is expressed as the relative luminescence calculated as the ratio of luminescence produced by Firefly luciferase to the luminescence produced by Renilla luciferase C) MKK3 modulates MYC activity to control expression of cell cycle regulating genes. The level of CDK4, CCND2, and CDKN1B was determined by western blot analysis of HCT116 cells expressing Venus-Flag fusions of MKK3 and MKK3 121–135. Flag-Venus

served as a background control. GAPDH was used as a loading control. Overexpression of both, MKK3 and MKK3 121–135 correlate with increased level of CDK4 and CCND2 and decreased level of CDKN1B comparing to the Venus control. D) Quantitative reverse-transcriptase PCR (qRT-PCR) analysis revealed the upregulation of CDK6 and downregulation of CDKN2A in HCT116 cells overexpressing Venus-Flag-tagged MKK3 or MKK3 121–135. Venus-Flag-ERK1 served as a positive control. The mRNA expression level is represented as the fold change of each mRNA normalized to GAPDH and relative to Flag-Venus control. E) Working model. In addition to the established MKK3/p38 pathway, MKK3 may regulate MYC activity through a direct physical protein-protein interaction.

Author Manuscript

Author Manuscript

Author Manuscript

Author Manuscript